Research Article Vol. 27, No. 25 / 9 December 2019 / Optics Express 36276

Optics EXPRESS

# Robust inverse-design of scattering spectrum in core-shell structure using modified denoising autoencoder neural network

**BAIQIANG HU,[1] BEI WU,[1] DONG TAN,[1] JING XU,[1,2] AND YUNTIAN CHEN[1,2,*]**

[1] *School of Optical Electronic Information, Huazhong University of Science and Technology, Wuhan 430074, China*
[2] *Wuhan National Laboratory for Optoelectronics, Huazhong University of Science and Technology, Wuhan 430074, China*
[*] *yuntian@hust.edu.cn*

**Abstract:** Neural network–based inverse design of nanophotonic device network is computationally and time efficient, but in general suffers the problems of robustness and stability against variation of the input target electromagnetic response. The inverse design network is required to be robust against the input electromagnetic response and to be capable of approximating the given electromagnetic response, even under the circumstances that the exact target response may not exist. We introduce a modified denoising autoencoder network to ensure the robustness of neural network–based inverse design, which consists of (1) a pre-trained network as a substitute of numerical simulation and (2) an inverse design network. We further purposely train the network with certain random disturbances added to the training dataset generated by the pre-trained network. Consequently, our modified denoising autoencoder network is more robust and more accurate than the conventional fully connected neural network. The strength and flexibility of our proposed network is illustrated via three concrete examples of achieving the desired scattering spectra of layered spherical scatterers.

## 1. Introduction

The inverse design of nanophotonic devices is highly important, as evident by recent work [1–19]. The conventional inverse design and optimization of nanophotonic devices contain the evolutionary method (genetic algorithm and particle swarming optimization [20]), the gradient-based method (topology optimization [21–23] and steepest descent [24]), and other methods based on heuristics (simulated annealing [25]). These techniques can open up the full parameter space and obtain many non-intuitive designs, but need prior knowledge as the starting point for the iteration and become more computationally expensive and time inefficient as structural complexity grows.

In contrast to the time efficiency and computational overload of the aforementioned methods, artificial intelligence in the past few years develops rapidly and is promising in solving the inverse design problems of nanophotonic devices. In particular, neural network (NN) based machine learning techniques play an important role in the inverse design of nanophotonic problems, as studied in recent literature [3,4,10–19,24,26–32]. Peurifoy et al. optimized structural parameters using NN model trained in advance as a substitute of electromagnetic simulator [17]. Liu et al. used tandem NN to directly solve the inverse design problem of optical thin films [29], which avoided the nonuniqueness problem and obtained a well converged NN in the inverse design problem by cascading a pre-trained auxiliary network. Those works using NNs have a potential problem, which is related with the robustness of the target responses, especially

#376837 https://doi.org/10.1364/OE.27.036276
Journal © 2019 Received 10 Sep 2019; revised 14 Nov 2019; accepted 16 Nov 2019; published 26 Nov 2019

under circumstances where the target responses may not be the true solutions of the Maxwell's equations.

In fact, the robustness in all types of inverse design problems is crucial, as evident by the following facts. Firstly, the target response is not known in advance, and occasionally too ideal to be a valid solution of the Maxwell's equations. Provided that we give a set of target responses arbitrarily, there may be no corresponding structures and thus the NN based inverse design is very likely to fail because NN itself is very sensitive to the input data. Secondly, NN is not suitable for robust inverse design due to the incompatibility between the basic assumptions of NNs and the data distribution of inverse problems. The distribution of the input data in the parameter space is considered to be evenly distributed, with an implicit assumption that the testing data point can be obtained by interpolating some known data points. However,the interpolation of two already known electromagnetic responses usually may not exist, these render the stability of the NN based inverse design extremely challenging.

In this paper, we propose a modified denoising autoencoder network (MDAN for short) by introducing dual learning strategy to the denoising autoencoder NN [33]. Firstly, we use the original training dataset to train a forward design network (forward net for short) with very high accuracy as a substitute of electromagnetic simulator, thereby we can extract the full capability of the original dataset and take advantage of forward net to generate the new dataset of the unlabeled structures. Secondly, an inverse design network (inverse net for short) is cascaded behind the forward net to form an autoencoder-like network. As such, the training set for the inverse design is not the same as the original training dataset, but generated by the forward net instead. It is worthy to point out that the two nets function as an image to each other, which is essential in the dual-learning process. Once the whole network is well trained, the inverse net can fully explore the electromagnetic response space interpolated by the forward net. Thirdly, we perturb the new dataset for the inverse net by adding random noise on the spectra to make the network more robust. The high frequency components of the spectrum curves are more affected by the added noise than the low frequency components. This allows the NN to focus on learning the low frequency components, leading to a smoother weight matrix in the NN. Consequently, a higher performance of generalization ability and robustness of the MDAN is achieved.

The paper is organized as follows. In Section 2, we give a brief description of the realization of the MDAN. In Section 3, we compare the convergence of loss function and the robustness of the fully connected neural network (FCNN for short) and the MDAN for a specific scattering problem. We find that the MDAN is more robust and has lower value of loss function compared with that of the FCNN. As an example, we use the MDAN to solve an inverse scattering problem with target responses of double peaks and single peak scattering spectra and far-field radiation, which indeed yields robust and meaningful geometric parameters of the desired structures. Finally, Section 4 concludes the paper.

## 2. The inverse design neural network: FCNN and MDAN

The FCNN is a relatively simple NN, which has a good performance in predicting the optical responses of the specific nanophotonic structures in terms of accuracy and simplicity. However, the FCNN has difficulty in dealing with the inverse design of the nanophotonic devices, as evident in the aforementioned discussion. Here, the FCNN is considered as a reference network for inverse design problems, as shown in Fig. 1(a), which consist of an input layer, an output layer and a number of hidden layers in-between. The input layer stands for the optical responses represented by a vector $[S_i]$, and the output layer stands for the geometric parameters of the nanophotonic devices represented by a vector $[R_j]$. Specifically, the inverse design training with the FCNN is trained using Adam optimizer and its loss function is the mean square error (MSE). In general, the inverse design of nanophotonic devices encounters a few crucial difficulties, especially the robustness problem as discussed previously. The goal of this paper is to propose the MDAN to solve the robustness problem of nanophotonic devices inverse design. Our MDAN consists of two sub-network, i.e., the forward net and the inverse net, as shown Fig. 1(b).

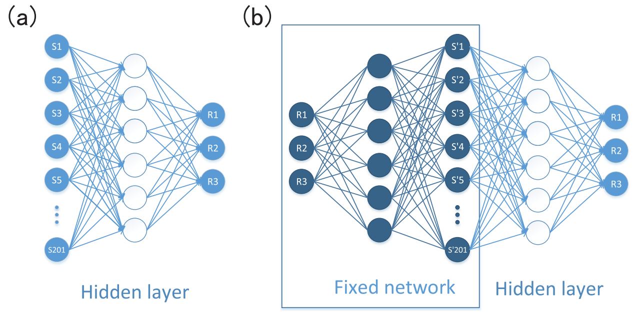

**Fig. 1.** Architecture diagram of (a) FCNN and (b) MDAN. In the MDAN, there are fixed forward net (dark blue) and the inverse net (blue), cascaded with each other.

The working principle of constructing the MDAN is given as follows. Firstly, the forward net is a FCNN, but pre-trained with the original dataset. Once the pre-training is converged, the network weights and biases of the forward net are fixed, and subsequently the fixed forward net functions as a data generator for the inverse net. Importantly, the forward net provides an access to the original dataset that can be fully explored by the inverse net, and thus a seamless connection between the original dataset and the inverse net is established. Secondly, the inverse net is structurally identical to the reference FCNN, and is cascaded behind the fixed forward net, as shown in Fig. 1(b). By concatenating the forward net and the inverse net together, our NN can be considered as a partially fixed autoencoder network. The random structures are fed to the whole network, where only the inverse net are updated iteratively until the whole network is converged. As such, the inverse net is easier to obtain the convergence without overfitting, in comparison with the reference FCNN in Fig. 1(a). Moreover, the proposed MDAN, as well as other modified versions of autoencoder NN, can also avoid the nonuniqueness problem in the inverse design, as discussed in details by Liu and her/his co-workers [29]. Thirdly, the idea of denoising autoencoder NN is introducing certain amounts of noise to improve the robustness performance of the NN. With partially corrupted input data fed to the inverse net, the weights distribution is smoother than that trained by the original dataset, and the low-dimensional components of the input data are more robust against the added noise. Importantly, one can achieve a better balance between accuracy and robustness using the MDAN compared to those using the FCNN by carefully adjusting the amount of noise added to the training dataset. As such, meaningful optimal nanophotonic geometric parameters can be obtained eventually, even under the circumstances where the target optical response may not be a valid solution of the Maxwell's equations.

## 3. Results and discussions

### 3.1. *The inverse design of core-shell structure*

Multi-layered spherical nanoparticles are known to be able to achieve large electric field enhancements via highly resonant electrically small geometries [34]. As shown in Fig. 2(a), we consider an isolated multi-layer core-shell nanoparticle, which consists of Au, Ag, $TiO_2$ layers embedded in air. Provided a given scattering spectrum, the inverse scattering problem is aimed to output the geometric parameters of the core-shell nanoparticle that yields the optimal overlapped spectrum with the target response. Specifically, we consider a target response of the core-shell nanoparticle with double peaks (380 nm & 625 nm) to improve the performance of phosphor quantum dots (QDs) based light-emitting diodes, where the QDs have the absorption peak at 380 nm and the emission peak at 625 nm [35].

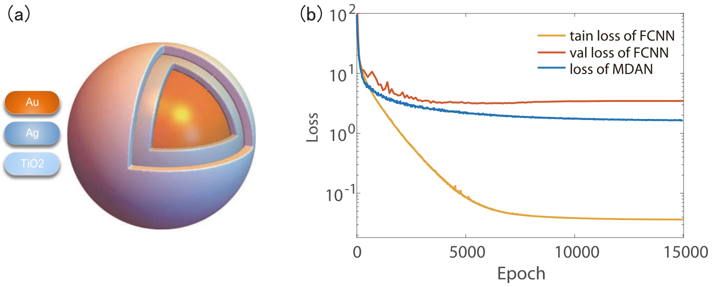

**Fig. 2.** (a) The core-shell spherical nanoparticle consists of Au, Ag, $TiO_2$ layers, and the hosting medium is air. (b) Loss function of the FCNN and the MDAN is plotted as a function of epoch. The final loss of the MDAN is higher than the the training loss, but lower than validation loss of the FCNN.

In the following, we train two networks, the FCNN and the MDAN, to solve the inverse scattering problem shown in Fig. 2(a). The training instance is given as follows, 201 sampling points of the scattering spectrum ($[S1, S2, \ldots, S201]$) with the wavelength ranging from 300 nm to 700 nm, and the output thicknesses of three layers (Au, Ag, $TiO_2$) of the core-shell structure ($[R1, R2, R3]$) are set in the range of 5 nm - 55 nm. The structure of the FCNN is 201-400-300-200-100-3, corresponding to the number of neurons in the six layers respectively. The input layer matches the spectrum vector $[S1, S2, \ldots, S201]$, while the output layer yields the thicknesses vector $[R1, R2, R3]$. Regarding the MDAN, the pre-trained fixed forward net is a FCNN with Adam optimizer and a loss function of MSE, which consists of six layers with 3-100-200-300-400-201 neurons, respectively. The inverse net can be considered as a mirror image of the fixed forward net, and the whole network is trained similar to the autoencoder network. The original dataset is obtained by solving Mie scattering of the core-shell nanoparticle [36]. The full dataset consists of (1) training set of 5000 instances(the validation set is included), and (2) the test set of 1000 instances. The number of instances in this dataset is relatively small compared to the others' works due to the fact that the parameter space of structure is set to be small to alleviate effect of the non-uniqueness problem, and with the data generator we can employ the unlabeled dataset to obtain a better accuracy performance.

### 3.2. Robustness performance of MDAN and FCNN

We consider a concrete example to illustrate the robust inverse design of the core-shell structure based on the MDAN. To this end, we first examine the performance of the loss functions of the FCNN and the MDAN, which are fully trained under the similar hyper-parameters (batch/epoch size is 200/15000 for the FCNN, epoch size is 15000 for the MDAN, and the batch size of the MDAN is not well defined) such that the loss functions eventually reach stable values. Figure 2(b) shows the comparison of loss function in the FCNN and the MDAN. Evidently, the validation loss is higher than training loss, which indicates that the FCNN occurs overfitting phenomenon on solving the inverse scattering problem. In contrast, the new dataset of the inverse net in the MDAN is real-time generated by the fixed forward network, thus there is no need for validation set. Though the original dataset fed to the forward net in the MDAN and the FCNN is the same, and a certain amount of noise is added to the training process in the MDAN, the final loss of MDAN is still lower than the validation loss of the FCNN for a large number epoch as shown in Fig. 2(b), showing that the MDAN converges better than the FCNN.

Next, we consider the robustness performance of the MDAN and the FCNN for the inverse design of core-shell structure by testing certain desired scattering spectra, i.e., the ratio of the scattering cross section to the cross-sectional area of the core-shell nanoparticle $Q_{sca}$. Specifically, we examine the similarity between the corresponding scattering spectra of the designed structures (designed spectra for short) and the target scattering spectrum (target spectra for short), as shown in Fig. 3, the designed structures are obtained through the two NNs by processing the target spectra with several disturbance (disturbed spectra for short), and the designed spectra are obtained through solving Mie scattering with the designed structures.

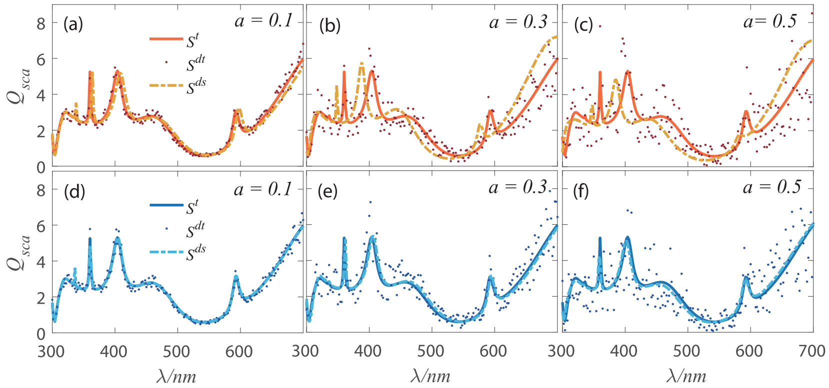

**Fig. 3.** (a)–(c)/(d)–(f) shows the scattering spectra as functions of wavelength for the FCNN/MDAN. The target spectra $S^t$ for the FCNN/MDAN are plotted with solid orange/blue lines, the disturbed spectra $S^{dt}$ with added noise for the FCNN/MDAN are plotted with dotted orange/blue lines, the design spectra $S^{ds}$ for the FCNN/MDAN are plotted with dashed orange/blue lines. $Q_{sca}$ represents the scattering efficiency.

Provided the target spectra $S^t$ (solid lines) plotted as function of wavelength $\lambda$ in Fig. 3, the disturbed spectrum $S^{dt}$ (dotted lines) is given by $S^{dt} = (1 + a\varepsilon)S^t$, where $a$ quantifies the magnitude of the added noise, and $\varepsilon$ is a random value evenly distributed in the interval $[-1, 1]$. The disturbed spectra $S^{dt}$ are fed to the MDAN and the FCNN for the inverse design, which output the geometric parameters of the designed structures. Then by directly solving the Mie scattering with those geometric parameters, the corresponding designed spectra $S^{ds}$ are obtained and plotted as the dashed lines in Fig. 3. For the FCNN, as shown in Figs. 3(a)–3(c), when $a \geq 0.3$, the FCNN fails to perform the inverse design, since the designed spectrum $S^{ds}$ and the target spectrum $S^t$ deviates significantly. In a sharp contrast, as $a$ is increased from 0.1 to 0.5, $S^{ds}$ of the MDAN hardly deviates from $S^t$ as shown in Figs. 3(d)–3(f). Such high tolerance indeed indicates that the MDAN is more robust against the input spectrum corruption than that of the FCNN. Importantly, for a given target response that may not exist, the MDAN yields an output which has a most optimal spectrum compared with the target response, while the FCNN fails completely. In practice, there are plenty of examples of such failures in the NN based inverse design-like problem due to the lack of the robustness or tolerance to the network input. For an example in the field of image recognition, the NN usually outputs meaningless results even if only a small fraction of disturbance is added to the input [37].

The discussions above vividly depict the difference of robustness in both network only for single instance. And though the non-uniqueness problem is not our focus in this paper, its effect on the structural relative error should be considered as well. In the following, we will discuss the robustness of the inverse design by comparing the effects of different noise magnitudes on structural relative error using the FCNN and the MDAN on the whole test set. To that end, we first define the relative error for the $i$th instance in the test set, i.e., $err_r^i(a) = \frac{r^{ds}(a)-r^t}{r^t}$, where $r^{ds}(a)$

is the thickness of the designed core-shell structure, obtained from two inverse design networks with disturbed spectrum $S^{dt}(a)$, $a$ ranging from 0.1 to 0.5 is the magnitude of the noise, $r^t$ is the thickness of the target core-shell structure corresponding with the target spectrum $S^t$ . The total relative error over all the instances in the test set is further defined as $err_r^{total}(a) = \frac{1}{N}\sum_i err_r^i(a)$, where $N = 1000$ is the size of test set in this paper. Though the added random noise has a fixed magnitude $a$, the output $r^{ds}(a)$ will be slightly different. Hence, we test the NNs ten times and take the mean value as the average relative error $err_r^{ave}(a) = \frac{1}{10}\sum err_r^{total}(a)$, which are the data points plotted in Fig. 4. Notably, $err_r^{ave}(a)$ is a three-component vector, which consists of the average errors of Au, Ag, and $TiO_2$ layers in the core-shell structure.

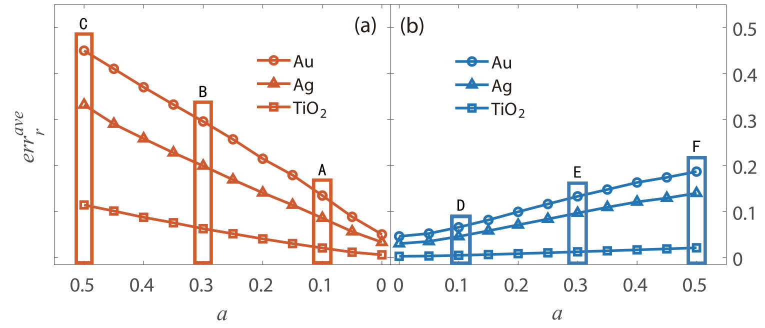

**Fig. 4.** (a)–(b) shows the average relative error $err_r^{ave}$ of the structure as function of $a$ for the FCNN/MDAN. The three lines marked with circle, triangle and square represent the $err_r^{ave}$ of the Au, Ag, $TiO_2$ layers. The six inset box marked as A-F are corresponding to the panels as shown in in Figs. 3(a)–3(f), respectively.

Figure 4(a) shows the average relative error $err_r^{ave}$ as a function of noise magnitude $a$ for the FCNN. Evidently, $err_r^{ave}$ grows rapidly as $a$ increases. Especially, $err_r^{ave}$ of the Au layer reaches almost 50% with $a = 0.5$. While in the Fig. 4(b), it is clearly seen that $err_r^{ave}$ of the MDAN grows slowly as $a$ increases and its maximum is less than 20%. Interestingly, $err_r^{ave}$ of $TiO_2$ is smaller than those of Au and Ag layers in both networks. This is due to the following facts: (1) Au and Ag layers have certain similar optical properties which lead to the non-uniqueness problem, thus some certain different pairs of Au and Ag thickness with the same $TiO_2$ thickness may result in very similar electromagnetic responses. For example, the two sets of geometric parameter vectors $[R1, R2, R3]$, i.e., the first set given by [21.3, 31.2, 54.1] nm and [33.3, 18.6, 54.1] nm, and the second set given by [15.8, 45.4, 26] nm and [31.9, 29.5, 26] nm, both have almost completely overlapping spectra; (2) Though easier to converge, the autoencoder-like network, the MDAN as mentioned above, still does not solve the non-uniqueness problem thoroughly. For some similar target spectra $S_1^t$ and $S_2^t$ which correspond to distinct structure parameters, for example [21.3,31.2,54.1] nm and [33.3 18.6 54.1] nm, it is hard for the inverse net to identify which is the correct one. Feeding different disturbed spectra $S^{dt}$ based on $S_1^t$ (or $S_2^t$), the inverse net outputs these two structure parameter vectors randomly, especially the parameters for the Au and Ag layers. But for the $TiO_2$ layer, different thicknesses correspond to different spectra, so the network can obtain accurate value of the $TiO_2$ layer's thickness.

### *3.3. Inverse design of targeted single peak and double peaks spectrum*

Three examples shown in Fig. 5 are illustrated to validate our proposed MDAN for the inverse design of core-shell nanoparticle, in comparison with the results obtained from the FCNN. The target spectra are not valid solutions of Maxwell's equations but designed with Gaussian distribution.

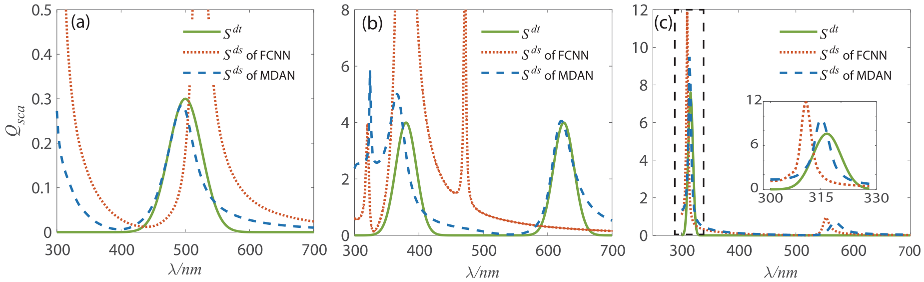

**Fig. 5.** (a)–(b)–(c) shows the single peak/ double peaks/ sharp peak target spectrum $S^t$ and the designed spectrum $S^{ds}$ obtained by the FCNN and the MDAN.

In Fig. 5(a), we consider an idea target spectrum (solid line), i.e., a single peak Gaussian distribution $S^t(\lambda) = q \cdot e^{-\frac{(\lambda-\mu)^2}{2\sigma^2}}$, with the wavelength $\lambda \in [300, 700]$, the expected value $\mu = 500$, the standard deviation $\sigma = 26$ and the magnitude of the scattering efficiency $q = 0.3$. By feeding this spectrum to the MDAN, the output structure with the parameter vector [11.3, 8.5, 6.5] nm yields Gaussian-like spectrum $S^{ds}$ plotted as the dashed line, which is well overlapped with $S^t$. And for the FCNN, the design structure has the thickness vector of [13.1, 9.2, 10.3] nm, whose corresponding $S^{ds}$ (dotted line) has a significant deviation from the target spectrum $S^t$.

In Fig. 5(b), the target spectrum $S^t$, i.e., the sum of two Gaussian distributions is inversely designed by both networks. Each of the Gaussian function has the same standard deviation $\sigma = 16$ and the amplitude parameter $q = 4$, but the different expected value at $\mu_1 = 380$ and $\mu_2 = 625$. As for the MDAN, the thickness vector of the output design structure is [29.4, 6.2, 24.1] nm and the corresponding design spectrum $S^{ds}$ (dashed line) is well overlapped with the target spectrum $S^t$ (solid line) of double peaks Gaussian curves. In contrast, the vector of design structure obtained from the FCNN is [28.2, -103.4, 44.9] nm (which of course does not even exist in reality), the design spectrum of which also fails completely, but it is still illustrated for consistency, plotted as dotted line in Fig. 5(b).

In Fig. 5(c), the target spectrum (solid line) is a sharp Gaussian distribution with the expected value $\mu = 316$, the standard deviation $\sigma = 4$ and the max magnitude of the scattering efficiency $q = 7.6$. By feeding this curves to the both network, the output structures are [12.14, 7.52, 16.96] nm for the MDAN and [1.31, 14.37, 17.81] nm for the FCNN, and the $S^{ds}$ are plotted with dashed and dotted line respectively. The $S^{ds}$ of MDAN is well overlapped with $S^t$ and the $S^{ds}$ of FCNN is also a single peak with the peak point deviates slightly from the target spectrum $S^t$, but the structure parameter is out of meaningful range, which is set to be [5, 55] nm.

As can be seen from above, even if the target spectrum is not a valid solution of the Maxwell's equations, the MDAN is still able to output a meaningful design structure with a valid and optimal overlapping design spectrum, while the FCNN fails to output a proper and meaningful geometric parameters of the core-shell design structures.

### 3.4. Inverse design of far-field radiation of asymmetric eccentrical core-shell structure

We apply the MDAN to a more sophisticated scenario, which is the inverse design of far-field radiation of the asymmetric eccentrical core shell structure. As shown in Fig. 6(a), we consider an asymmetric two-layer core-shell element, with $\varepsilon_1$=3 and $\varepsilon_2$=8. The wavelength $\lambda$ is set at 633 nm. A specific structure is characterized by parameters $[r_1, r_2, b_1, b_2]$ , $r_1$ and $r_2$ represent the radii of the outer and inner circles, $b_1$ and $b_2$ represent distances between centers of two circles. The Fig. 6(b) shows the far-field radiation with azimuthal angle ranging from 0 to 360. Since the relative positions of the two circles are randomly given, the analytical Mie theory is not directly applicable. Therefore, the Green Function method is used to calculate the far-field radiation of the asymmetric structure [38] for preparing the training data set. The training set consists of 5000 instances. The input of the network is the far-field radiation discretized to 361 points and the output label is $[r_1, r_2, b_1, b_2]$, where $r_1$, $r_2$, $b_1$ and $b_2$ are in the range of $[100, 300]$ nm, $[500, 700]$ nm, $[-200, 200]$ nm and $[-200, 200]$ nm, respectively.

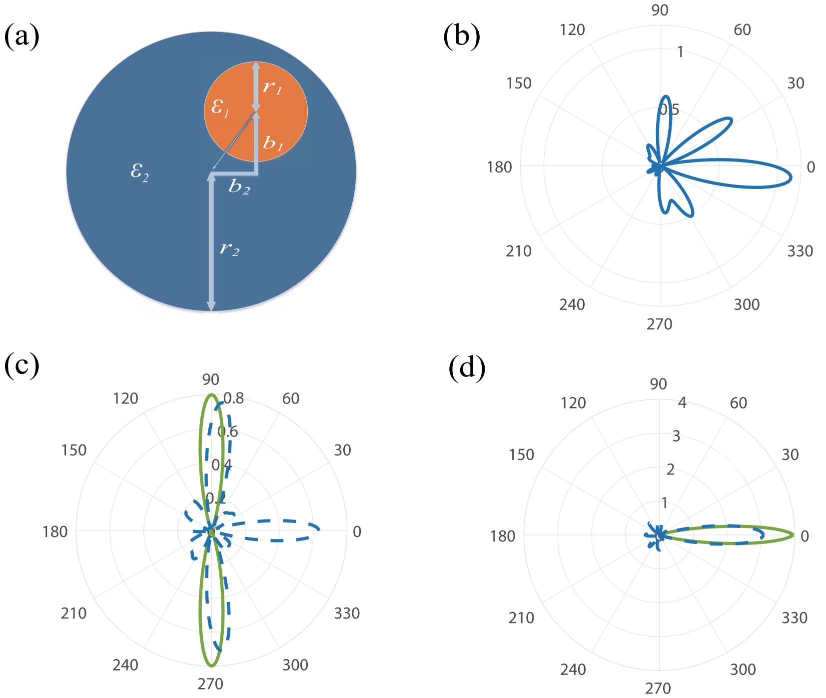

**Fig. 6.** (a) The asymmetric eccentrical core-shell structure is characterized by $\varepsilon_1$, $\varepsilon_2$, $r_1, r_2, b_1, b_2$ and the hosting medium is air; (b) shows a standard far-field radiation; (c) and (d) shows the inverse design of double peaks and single peak target far-field radiation.

In the training process, the MDAN and FCNN share the same hyperparameters as much as possible. The FCNN has a poor convergence with a relative error larger than 20%, thus the inverse design of far-field radiation can only be implemented by the MDAN. Similar to previous work, the double peaks and single peak patterns are used as the target response for inverse designing. In Fig. 6(c), the target far-field radiation contains two Gaussian peaks as $S^t(\text{deg}) = q \cdot e^{-\frac{(\text{deg}-\mu)^2}{2\sigma^2}}$ with the deg in $[0, 360]$, the $\sigma$ is the standard deviation, the $\mu$ is the expected value and the $q$ is the magnitude parameter. Each Gaussian peaks in the double peaks target far-field radiation has the same $\sigma = 8$ and $q = 0.8$, but the different $\mu_1 = 90$ and $\mu_2 = 270$. By feeding this spectrum to the MDAN, the output design structure is [202.7, 596.8, -8.9, -65.9] nm and the corresponding design spectrum $S^{ds}$ (dashed line) is relatively well overlapped with the target spectrum $S^t$ (solid line) of double peaks Gaussian curves. The main scattering lobe cannot be eliminated for the given materials and structures. In Fig. 6(d), the target far-field radiation is dominated by a single Gaussian peak. The expected value is splitted to $\mu = 0$ and $\mu = 361$, the standard deviation is $\sigma = 7$, and the magnitude of the far-field radiation is $q = 4$. By feeding this spectrum to the MDAN, the output design structure is [187.3, 557.3, 0.3, 23.2] nm, and the designed far-field radiation is plotted as the dashed line, which contains most of the scattering energy in the main lobe.

As a concluding remark, our proposed MDAN has a dual structure that is similar to the autoencoder network and a denoising procedure inspired by denoising autoencoder. The dual structure of data generation and data learning makes it possible for the inverse design network to learn from the generated data by forward net rather than only from the raw data. The denoising procedure forces the NN to discard the high-frequency components in the data set and retain the pure features of better generalization performance by adding controlled noise, thus the tolerance of the NN to data corruption is improved. By introducing the dual structure of network and input corruptions, the MDAN gets a higher performance in accuracy and robustness compared with the reference FCNN.

## 4. Conclusion

In conclusion, we address the robustness problem in the NN based inverse design method. Specifically, we propose a generative and mirrored network, i.e., our MDAN, to realize the direct inverse design of nanophotonic devices inspired by the architecture of the denoising autoencoder network. The inverse design of the MDAN can handle multiple input spectra without reducing efficiency. This model is readily extended to convolutional neural network for more complicated photonics inverse design, such as mode multiplexer and demultiplexer.

## Funding

National Natural Science Foundation of China (11874026, 61735006, 61775063); Fundamental Research Funds for the Central Universities (HUST: 2017KFYXJJ027, HUST:2018KFYYXJJ055); National Basic Research Program of China (973 Program) (2017YFA0305200).

## Disclosures

The authors declare no conflicts of interest.

## References

1. W. Chang, M. Zhang, L. Lu, F. Zhou, D. Li, Z. Pan, and D. Liu, “Inverse design of an ultra-compact mode (de) multiplexer based on subwavelength structure,” in *CLEO: Science and Innovations*, (Optical Society of America, 2017), pp. SF1J-8.
2. W. Chang, X. Ren, Y. Ao, L. Lu, M. Cheng, L. Deng, D. Liu, and M. Zhang, “Inverse design and demonstration of an ultracompact broadband dual-mode 3 db power splitter,” Opt. Express **26**(18), 24135–24144 (2018).
3. S. Molesky, Z. Lin, A. Y. Piggott, W. Jin, J. Vucković, and A. W. Rodriguez, “Inverse design in nanophotonics,” Nat. Photonics **12**(11), 659–670 (2018).
4. I. Malkiel, A. Nagler, M. Mrejen, U. Arieli, L. Wolf, and H. Suchowski, “Deep learning for design and retrieval of nano-photonic structures,” arXiv preprint arXiv:1702.07949 (2017).
5. S. So, J. Mun, and J. Rho, “Simultaneous inverse design of materials and structures via deep learning: Demonstration of dipole resonance engineering using core-shell nanoparticles,” ACS Appl. Mater. Interfaces **11**(27), 24264–24268 (2019).
6. J. A. Fan, “Generating high performance, topologically-complex metasurfaces with neural networks,” in *CLEO: Applications and Technology*, (Optical Society of America, 2019), pp. AM4K-4.
7. E. W. Wang, D. Sell, T. Phan, and J. A. Fan, “Robust design of topology-optimized metasurfaces,” Opt. Mater. Express **9**(2), 469–482 (2019).
8. D. Z. Zhu, E. B. Whiting, S. D. Campbell, P. L. Werner, and D. H. Werner, “Inverse design of three-dimensional nanoantennas for metasurface applications,” in *2019 International Applied Computational Electromagnetics Society Symposium (ACES)*, (IEEE, 2019), pp. 1–2.
9. S. D. Campbell, D. Sell, R. P. Jenkins, E. B. Whiting, J. A. Fan, and D. H. Werner, “Review of numerical optimization techniques for meta-device design,” Opt. Mater. Express **9**(4), 1842–1863 (2019).
10. L. H. Frandsen and O. Sigmund, “Inverse design engineering of all-silicon polarization beam splitters,” in *Photonic and Phononic Properties of Engineered Nanostructures VI*, vol. 9756 (International Society for Optics and Photonics, 2016), p. 97560Y.
11. A. Y. Piggott, J. Petykiewicz, L. Su, and J. Vučković, “Fabrication-constrained nanophotonic inverse design,” Sci. Rep. **7**(1), 1786 (2017).
12. T. Asano and S. Noda, “Optimization of photonic crystal nanocavities based on deep learning,” Opt. Express **26**(25), 32704–32717 (2018).

13. I. Malkiel, M. Mrejen, A. Nagler, U. Arieli, L. Wolf, and H. Suchowski, "Deep learning for the design of nano-photonic structures," in *2018 IEEE International Conference on Computational Photography (ICCP)*, (IEEE, 2018), pp. 1–14.
14. M. H. Tahersima, K. Kojima, T. Koike-Akino, D. Jha, B. Wang, C. Lin, and K. Parsons, "Deep neural network inverse design of integrated photonic power splitters," Sci. Rep. **9**(1), 1368 (2019).
15. J. Jiang, D. Sell, S. Hoyer, J. Hickey, J. Yang, and J. A. Fan, "Data-driven metasurface discovery," arXiv preprint arXiv:1811.12436v1 (2018).
16. K. Yao, R. Unni, and Y. Zheng, "Intelligent nanophotonics: merging photonics and artificial intelligence at the nanoscale," arXiv preprint arXiv:1810.11709 (2018).
17. J. Peurifoy, Y. Shen, L. Jing, Y. Yang, F. Cano-Renteria, B. G. DeLacy, J. D. Joannopoulos, M. Tegmark, and M. Soljačić, "Nanophotonic particle simulation and inverse design using artificial neural networks," Sci. Adv. **4**(6), eaar4206 (2018).
18. R. Pestourie, C. Pérez-Arancibia, Z. Lin, W. Shin, F. Capasso, and S. G. Johnson, "Inverse design of large-area metasurfaces," Opt. Express **26**(26), 33732–33747 (2018).
19. S. Inampudi and H. Mosallaei, "Neural network based design of metagratings," Appl. Phys. Lett. **112**(24), 241102 (2018).
20. N. Jin and Y. Rahmat-Samii, "Advances in particle swarm optimization for antenna designs: real-number, binary, single-objective and multiobjective implementations," IEEE Trans. Antennas Propag. **55**(3), 556–567 (2007).
21. F. Wang, J. S. Jensen, and O. Sigmund, "Robust topology optimization of photonic crystal waveguides with tailored dispersion properties," J. Opt. Soc. Am. B **28**(3), 387–397 (2011).
22. R. E. Christiansen, F. Wang, and O. Sigmund, "Topological insulators by topology optimization," Phys. Rev. Lett. **122**(23), 234502 (2019).
23. O. Sigmund and K. Hougaard, "Geometric properties of optimal photonic crystals," Phys. Rev. Lett. **100**(15), 153904 (2008).
24. A. Y. Piggott, J. Lu, K. G. Lagoudakis, J. Petykiewicz, T. M. Babinec, and J. Vučković, "Inverse design and demonstration of a compact and broadband on-chip wavelength demultiplexer," Nat. Photonics **9**(6), 374–377 (2015).
25. S. Kirkpatrick, C. D. Gelatt, and M. P. Vecchi, "Optimization by simulated annealing," Science **220**(4598), 671–680 (1983).
26. S. So, J. Mun, and J. Rho, "Simultaneous inverse design of materials and parameters of core-shell nanoparticle via deep-learning: Demonstration of dipole resonance engineering," arXiv preprint arXiv:1904.02848 (2019).
27. Y. Sun, Z. Xia, and U. S. Kamilov, "Efficient and accurate inversion of multiple scattering with deep learning," Opt. Express **26**(11), 14678–14688 (2018).
28. W. Ma, F. Cheng, and Y. Liu, "Deep-learning-enabled on-demand design of chiral metamaterials," ACS Nano **12**(6), 6326–6334 (2018).
29. D. Liu, Y. Tan, E. Khoram, and Z. Yu, "Training deep neural networks for the inverse design of nanophotonic structures," ACS Photonics **5**(4), 1365–1369 (2018).
30. Z. Liu, D. Zhu, S. P. Rodrigues, K.-T. Lee, and W. Cai, "Generative model for the inverse design of metasurfaces," Nano Lett. **18**(10), 6570–6576 (2018).
31. Y. Khoo and L. Ying, "Switchnet: a neural network model for forward and inverse scattering problems," arXiv preprint arXiv:1810.09675 (2018).
32. C. Forestiere, Y. He, R. Wang, R. M. Kirby, and L. Dal Negro, "Inverse design of metal nanoparticles' morphology," ACS Photonics **3**(1), 68–78 (2016).
33. P. Vincent, H. Larochelle, Y. Bengio, and P.-A. Manzagol, "Extracting and composing robust features with denoising autoencoders," in *Proceedings of the 25th international conference on Machine learning*, (ACM, 2008), pp. 1096–1103.
34. S. D. Campbell, J. Nagar, P. L. Werner, and D. H. Werner, "Multi-objective analysis of multi-layered core-shell nanoparticles," in *2017 XXXIInd General Assembly and Scientific Symposium of the International Union of Radio Science (URSI GASS)*, (2017), pp. 1–3.
35. Y. Chen, Y. Zhang, and A. F. Koenderink, "General point dipole theory for periodic metasurfaces: magnetoelectric scattering lattices coupled to planar photonic structures," Opt. Express **25**(18), 21358–21378 (2017).
36. W. Liu, J. Zhang, B. Lei, H. Ma, W. Xie, and H. Hu, "Ultra-directional forward scattering by individual core-shell nanoparticles," Opt. Express **22**(13), 16178–16187 (2014).
37. C. Szegedy, W. Zaremba, I. Sutskever, J. Bruna, D. Erhan, I. Goodfellow, and R. Fergus, "Intriguing properties of neural networks," arXiv preprint arXiv:1312.6199 (2013).
38. W. Li, D. Tan, J. Xu, S. Wang, and Y. Chen, "Finite element based green's function integral equation for modelling light scattering," Opt. Express **27**(11), 16047–16057 (2019).